論文 / 著書情報
Article / Book Information

Title	Electrical characterization of the North Anatolian Fault Zone underneath the Marmara Sea, Turkey by ocean bottom magnetotellurics
Authors	T. Kaya, T. Kasaya, S. B. Tank, Y. Ogawa, M. K. Tuncer, N. Oshiman, Y. Honkura, M. Matsushima
Citation	Geophysical Journal International, Vol. 193, No. 2, p. 664-677
Pub. date	2013, 5
DOI	http://dx.doi.org/10.1093/gji/ggt025
Copyright	This article has been accepted for publication in Geophysical Journal International (c): 2013T. Kaya,T. Kasaya,S. B. Tank,Y. Ogawa,M. K. Tuncer,N. Oshiman,Y. Honkura,M. Matsushima Published by Oxford University Press on behalf of Royal Astronomical Society. All rights reserved.

Geophysical Journal International

Geophys. J. Int. (2013) **193,** 664–677 doi: 10.1093/gji/ggt025

Electrical characterization of the North Anatolian Fault Zone underneath the Marmara Sea, Turkey by ocean bottom magnetotellurics

Tülay Kaya,[1,2] Takafumi Kasaya,[3] S. Bülent Tank,[2,4] Yasuo Ogawa,[2] M. Kemal Tunçer,[5] Naoto Oshiman,[6] Yoshimori Honkura[1,2] and Masaki Matsushima[1]

[1]*Earth and Planetary Science, Tokyo Institute of Technology, Tokyo,* 152-8551, *Japan. E-mail: tulayk@ymail.com*
[2]*Volcanic Fluid Research Center, Tokyo Institute of Technology, Tokyo,* 152-8551, *Japan*
[3]*IFREE, Japan Agency for Marine-Earth Science and Technology, Yokosuka,* 237-0061, *Japan*
[4]*Geophysics, Bogazici University, İstanbul,* 34684, *Turkey*
[5]*Geophysics, İstanbul University, İstanbul,* 34320, *Turkey*
[6]*Disaster Prevention Research Institute, Kyoto University, Kyoto,* 611-0011, *Japan*

Accepted 2013 January 22. Received 2013 January 21; in original form 2011 December 31

SUMMARY

The first magnetotelluric study in the Marmara Sea, Turkey, was undertaken to resolve the structure of the crust and upper mantle in the region, and to determine the location of the westward extension of the North Anatolian Fault (NAF) in the Çınarcık area. Long-period ocean bottom magnetotelluric data were acquired at six sites along two profiles crossing the Çınarcık Basin, where a significant increase in microseismic activity was observed following the devastating 1999 İzmit and Düzce earthquakes. 2-D resistivity models indicate the existence of a conductor at a depth of ∼10 km in the middle of both profiles along with a deeper extension into the upper mantle, implying the presence of fluid in the crust and partial melting in the upper mantle. The northern and southern boundaries of this conductor are interpreted to represent the northern and southern branches of the NAF in the Marmara Sea, respectively. These conductors have been previously identified farther to the east along the NAF, suggesting that the electrical characteristics of this fault are continuous from onland areas into the Marmara Sea. Microseismic activity in the Çınarcık area is located above the conductor documented here, and indicates a possible seismogenic role of crustal fluids present in the conductive zone. In comparison, resistive zones along the NAF may act as asperities that could eventually result in a large earthquake.

Key words: Magnetotelluric; Marine electromagnetics; Earthquake source observations; Fractures and faults; Kinematics of crustal and mantle deformation; Rheology: crust and lithosphere.

1 INTRODUCTION

The 1600-km-long North Anatolian Fault (NAF) is an intercontinental dextral strike-slip fault that is located between the northern Eurasian Plate and the southern Anatolian block (Fig. 1a). After closure of the Neo-Tethyan Ocean during the Late Mesozoic and Cenozoic, collision of the Arabian and Eurasian plates resulted in relative westward movement of the Anatolian Plate (McKenzie 1972; Toksöz *et al.* 1979). This westward movement is considered to be the main cause of major tectonic events along the NAF. During the past century, the epicentres of destructive earthquakes along the NAF have migrated westward starting with the 1939 Erzincan earthquake (M_s 7.9) and extending to the 1999 İzmit (M_w 7.4) and Düzce (M_w 7.2) earthquakes (Pınar *et al.* 2010). The fault rupture of the 1999 İzmit (M_w 7.4) earthquake extended into the Marmara Sea however, the fault segment between the 1912 Ganos and 1999 İzmit fracture zones (Fig. 1b) has not ruptured since 1766 (Toksöz *et al.* 1979); this segment in the Marmara Sea is considered to be a 'seismic gap' that may be capable of generating a $M \geq 7$ earthquake (Hubert-Ferrari *et al.* 2000).

The onland outcrop of the NAF is well known as a result of previous geological and geophysical studies (Ketin 1948; Barka 1992; Yılmaz *et al.* 1997; Akyüz *et al.* 2002; Şengör *et al.* 2005). Around the Marmara Sea, the NAF crosses three tectonic zones from north to south, with the northern zone consisting of Precambrian crystalline basement of the İstanbul–Zonguldak Zone, representing a south-facing Laurasian continental margin (Yılmaz *et al.* 1997). The southern zone, here termed the Sakarya Continent, is a

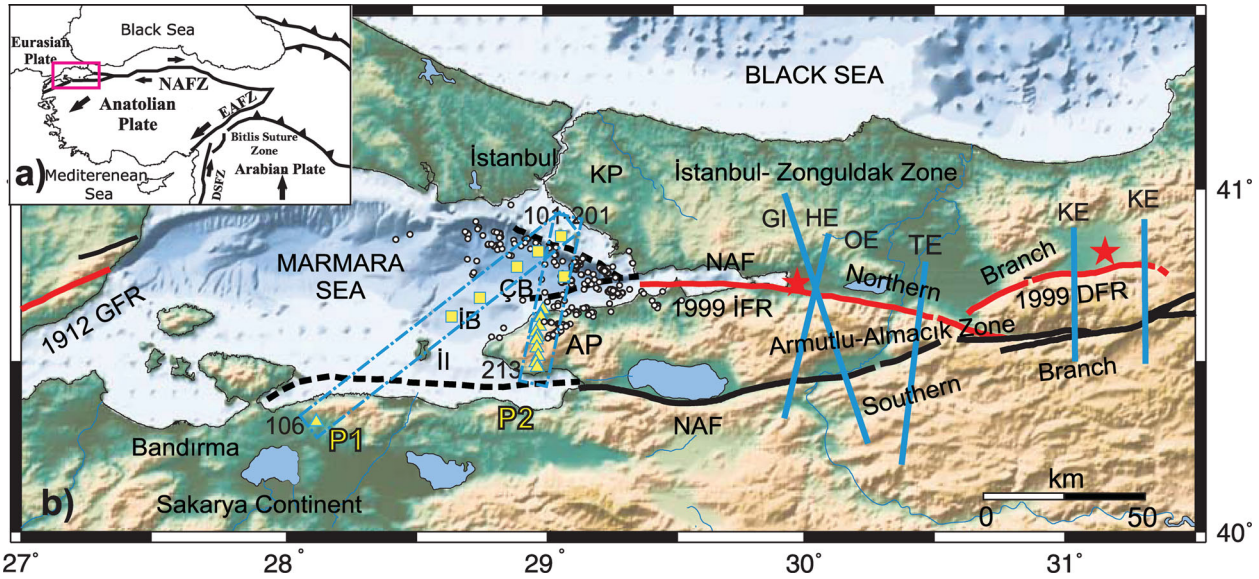

Figure 1. (a) Simplified tectonic map of Turkey, indicating the study area as delineated by a pink rectangle. Black lines and arrows indicate fault lines and plate motions in and around Turkey, respectively. (b) Location map of OBEM instruments (yellow squares) and MT (yellow triangles) sites within and around the Marmara Sea. Blue lines show previous MT profiles (GI, Gürer; HE, Honkura *et al.*; OE, Oshiman *et al.*; KE, Kaya *et al.*; TE, Tank *et al.*). Blue dashed rectangles show the location of the P1 and P2 profiles. The 1912 Ganos and the 1999 İzmit and Düzce earthquake ruptures are shown by solid red lines. Dashed black lines are possible traces of the NAF in the Marmara Sea. Red stars show epicentres of the 1999 İzmit and Düzce earthquakes. AP, Armutlu Peninsula; KP, Kocaeli Peninsula; ÇB, Çınarcık Basin; İFR, İzmit Fault Rupture; DFR, Düzce Fault Rupture; GFR, Ganos Fault Rupture; İI, İmralı Island; İB, İmralı Basin.

fragment of continental lithosphere that ruptured from Gondwanaland during the Triassic (Yılmaz *et al.* 1997). The Armutlu–Almacık Zone contains the remnants of the Intra-Pontide suture between the İstanbul–Zonguldak Zone and the Sakarya Continent, and consists of a tectonic melange of two zones (Fig. 1). All of these tectonic zones form constituent parts of the Western Pontides, a series of east–west trending Tethyan orogenic belts; this means that all three zones keep almost the entire evolutionary record of the Tethysides (Yılmaz *et al.* 1997). The occurrence of the İzmit and Düzce earthquakes on the northern side of these tectonic zones (Tank *et al.* 2003, 2005; Kaya *et al.* 2009; Tank 2012) indicates the significance of the extension of these zones into the Marmara Sea, in terms of possible locations for the next devastating earthquake along the NAF.

However, the juxtaposition of these zones beneath the Marmara Sea and the relationship between these zones and the NAF are currently poorly understood. A number of marine studies undertaken after the İzmit earthquake enabled the formulation of various tectonic models for the Marmara Sea, namely pull-apart (Armijo *et al.* 1999), single dextral strike-slip fault (Le Pichon *et al.* 2001), and extensional, crustal thinning models (Becel *et al.* 2009). The pull-apart model suggests that the Marmara Sea is a large pull-apart basin that includes a number of smaller pull-apart basins formed in a transtensional tectonic regime (Armijo *et al.* 2002). This model requires segmented faulting of the NAF within the Marmara Sea. According to Le Pichon *et al.* (2001), the NAF crosses the Marmara Sea as a single dextral strike-slip fault that follows the northern escarpment of the Çınarcık Basin (ÇB) in the east and cuts the Central Basin to the west. In comparison, crustal thinning model suggests the presence of an extensional regime in the Marmara Sea that is dependent on both normal and strike-slip faulting regime (Becel *et al.* 2009). Crustal thinning has been documented in the southern part of the Central Basin and is also observed beneath the İmralı and ÇBs (Laigle *et al.* 2008; Becel *et al.* 2009). The precise hypocentral distribution of microseismic activity (Bulut *et al.* 2009) is consistent with the down-dipping structures imaged by Carton *et al.* (2007) in the Marmara Sea and with present-day deformation controlled by a right-lateral strike-slip regime (Örgülü 2010). Local earthquake tomography (Karabulut *et al.* 2003; Barış *et al.* 2005) has imaged low *P*-wave velocity (*Vp*) and low *Vp*/*Vs* (where *Vs* = *S*-wave velocity) ratio zones down to 15 km depth beneath the Marmara Sea, in addition to high *Vp* and *Vp*/*Vs* ratio zones towards the northern and southern edges of the ÇB. Although previous studies have provided valuable information related to the form and tectonism of the NAF, the westward extension of this fault zone and the deeper structure beneath the Marmara Sea remain controversial.

Magnetotellurics (MT) is an electromagnetic method that utilizes naturally occurring electric and magnetic fields to map the subsurface electrical resistivity at depths ranging from the near surface to the upper mantle (Vozoff 1991). Since fluids significantly lower the electrical resistivity of rocks, this technique is highly useful in fault zone investigations (Ritter *et al.* 2005; Becken *et al.* 2011). Previous MT research undertaken around active fault zones indicates a strong correlation between the presence of fluids and seismic activity (Unsworth *et al.* 2000; Ogawa *et al.* 2001; Ogawa & Honkura 2004; Wannamaker *et al.* 2009; Becken *et al.* 2011), with the majority of fault zones being associated with resistor–conductor boundaries, and devastating earthquakes occurring in or around asperity zones identified by local resistive areas spatially associated with zones of low resistivity (Honkura *et al.* 2000; Oshiman *et al.* 2002; Tank *et al.* 2003, 2005; Kaya *et al.* 2009).

Previous onshore MT studies of the NAF have identified conductors at and below a depth of 10 km along the NAF, with northern and southern edges of the conductor coinciding with the surface traces of the NAF. The occurrence of main shocks and major aftershocks within brittle resistive zones (Tank *et al.* 2003, 2005; Kaya *et al.* 2009), and earthquake swarm activity around more ductile conductive regions (Tank *et al.* 2003) emphasizes the importance of fluids during seismic events. Our objective here is to image the western extension of the NAF under the Marmara Sea in an area known to be a seismic gap.

2 DATA

Fig. 1b shows the locations of magnetotelluric stations used during this study. We used 12 land sites (yellow triangles) and six ocean bottom sites (yellow squares) in the eastern part of the Marmara Sea, and defined two profiles (P1 and P2) for later 2-D modelling, as identified by dashed blue rectangles in the figure. The NE–SW oriented profile (P1) includes five ocean bottom sites, four of which are located in the Imralı and ÇBs, together with a single land site in the southern Marmara region. The second N–S oriented profile (P2) is composed of two ocean bottom sites and 11 land sites. The northernmost ocean bottom site is common in both profiles.

Ocean bottom magnetotelluric sites deployed during this study used ocean bottom electromagnetic instruments (OBEM) developed by Kasaya & Goto (2009). We measured two horizontal electric fields using 4 m dipoles with Ag–AgCl electrodes, and three-component magnetic fields using flux-gate sensors. The data were acquired with an 8 Hz sampling rate for about 3 weeks and all OBEM were successfully recovered after data acquisition. Time-series data acquired during deployment were analysed using a robust processing code (Chave *et al.* 1987) and usable MT transfer functions were obtained for a period range of 10–11 000 s, as shown in Figs 2 and 3.

Land site deployments during this study used broad-band Phoenix MTU5 MT instruments that cover a period range between 0.003 and 2000 s. However, in order to match the ocean bottom MT period range, data from the land MT sites were used at periods >10 s as shown in Figs 2 and 3. One land site at the southwestern end of profile P1 was a new deployment, with the other 11 land sites on profile P2 from Tank *et al.* (2003). These data were jointly inverted with the new ocean bottom data acquired during this study.

Figs 2 and 3 show the data obtained during this study as sounding curves, incorporating both diagonal and off-diagonal components. Fig. 2 shows observed data sounding curves across profile P1, comprising, from northeast to southwest, ocean bottom sites 101, 102, 103, 104 and 105 together with land site 106. The short period range ($<\sim$250 s) at sites 101, 102 and 103 contains clear phase rolling out of quadrant (PROQ; Chouteau & Tournerie 2000), with no such phase responses recorded at ocean bottom site 105. These differences can be explained by changes in bathymetry, with site 105 located on a shallow (50-m water depth), flat-lying section of seafloor, whereas the other ocean bottom sites are located near sharp changes in bathymetry. Electric currents in the ocean, perpendicular to bathymetric gradients, can generate secondary magnetic fields that are comparable to or even stronger than the primary magnetic field (Constable *et al.* 2009; Worzewski *et al.* 2010). Given this, the modelling discussed here did not incorporate short-period ocean bottom data that were affected by bathymetry-derived PROQ.

The dimensionality of the data set needs to be defined prior to 2-D or 3-D modelling. Here, we use the tensor-decomposition code of McNeice & Jones (2001), an expanded version of the Groom–Bailey decomposition (Groom & Bailey 1989) that incorporates multiple sites and periods, with strike directions inferred from the site- and period-dependent decomposition parameters shown in Fig. 4. The optimum strike directions in the 100–11 000 s period bands were N90°E and N62°E for profiles P1 and P2, respectively. These estimated 2-D strike directions were used to decompose the profile data, enabling the definition of TE and TM modes, which represent flows of electric current along and perpendicular to these strike directions.

3 MODELLING

We inverted the data by 2-D modelling using the appropriate strike directions defined within the preceding section. Although the strike directions along profiles P1 and P2 differ by some 28°, we assumed a quasi-2-D structure for the study area.

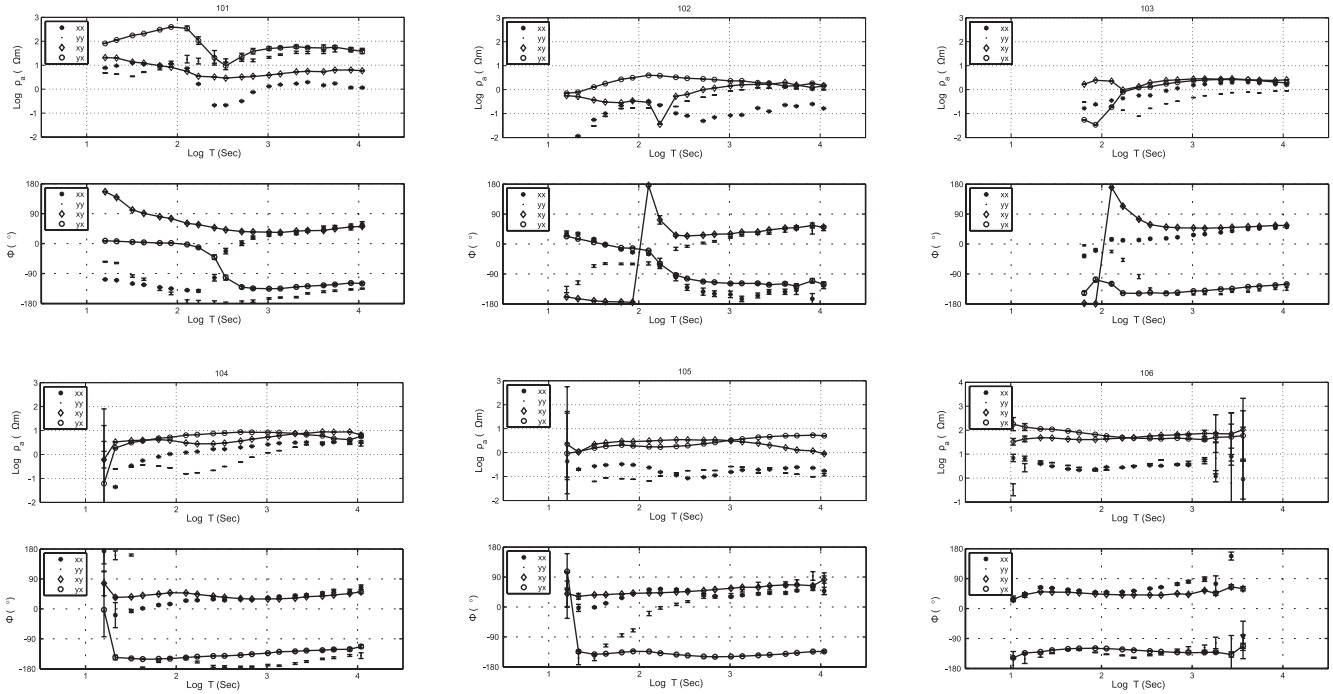

Figure 2. Observed apparent resistivity (Log ρ_a) and phase (Φ) values versus period (Log T) with their error bars estimated for XX (*), XY (-˙), YX (-○) and YY (□) components of the sites on P1. X and Y represent the north and east in coordinate system.

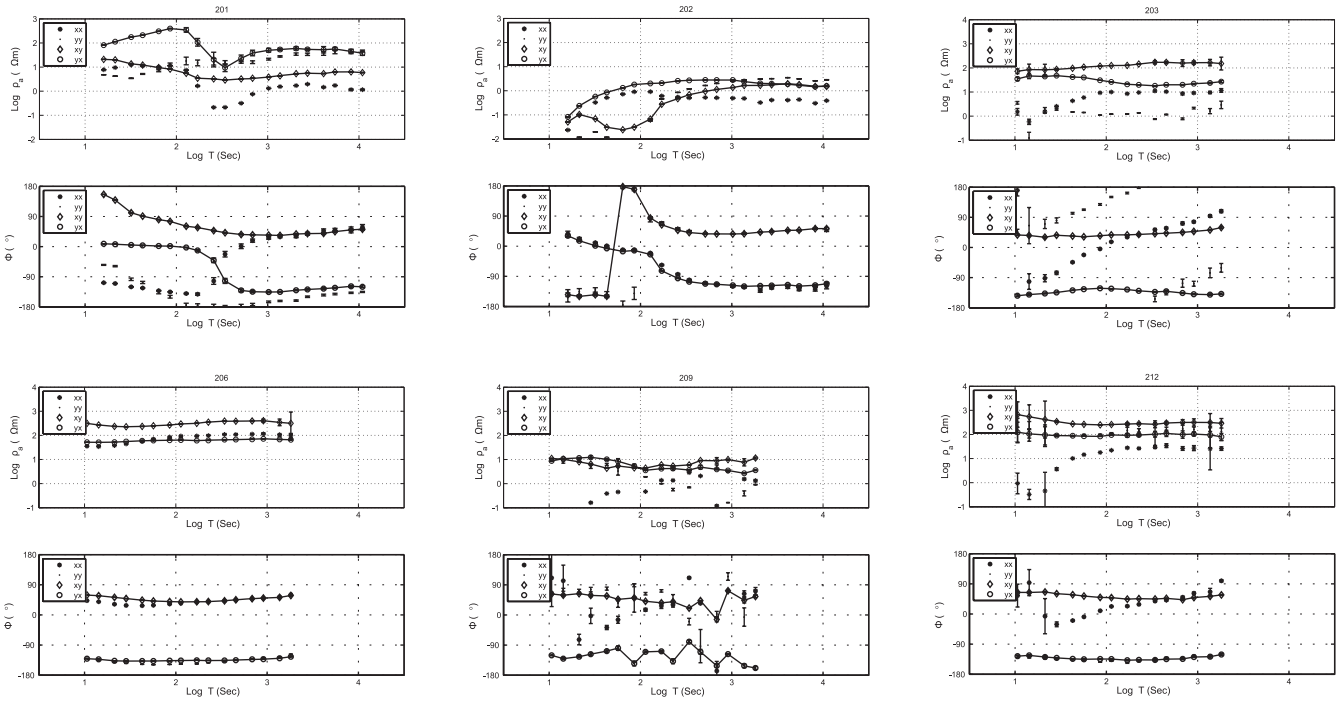

Figure 3. Observed apparent resistivity (Log ρ_a) and phase (Φ) values versus period (Log T) with their error bars estimated for XX (*), XY(-˙), YX (-○) and YY (□) components of the sites on P2. X and Y represent the north and east in coordinate system.

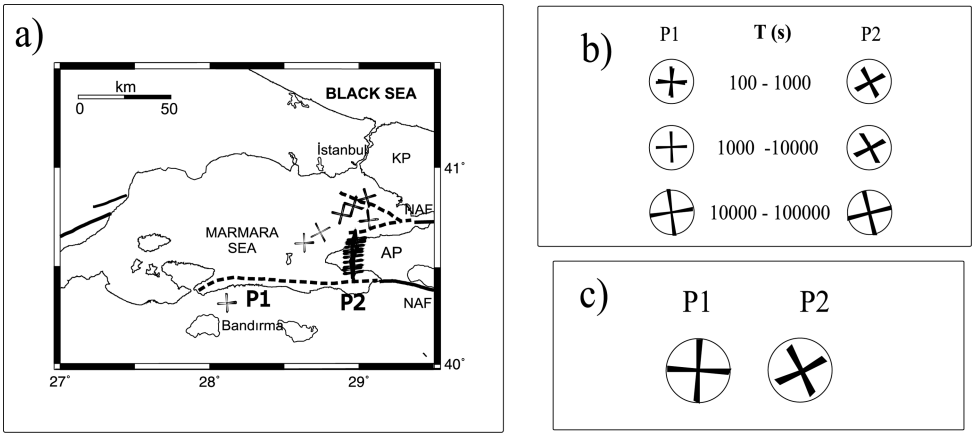

Figure 4. Site-dependent (a), frequency-dependent (b) and site- and frequency-independent (c) for the whole frequency range of 100–11 000 s strikes of P1 and P2.

It is known that TM mode 2-D modelling over a 3-D anomaly can robustly recover the resistivity section under the profile (Wannamaker *et al.* 1984). We tested such situation for an OBEM data set beneath the Marmara Sea. Fig. 5 shows a simplified 2-D and 3-D resistivity model that mimics the Marmara Sea; this model has a uniform earth of 100 Ωm and a box-shaped ocean of 0.3 Ωm with dimensions 180 km (E–W) × 60 km (N–S) × 1.2 km (depth). Fig. 6 compares the 2-D (Ogawa & Uchida 1996) and corresponding 3-D (Mackie *et al.* 1994) responses along the profile. The two northern stations (402 and 404) are on land, with the following two ocean bottom stations (406 and 408) close to the coast in the Marmara Sea, respectively. Solid lines denote 2-D TE (red) and TM (blue) responses, with asterisks denoting the corresponding 3-D responses. It is interesting to note that both TE and the corresponding 3-D responses have shorter period PROQ, primarily caused by the strong electrical current in the sea oriented parallel to the coastline, which can generate a large secondary horizontal magnetic field component with the opposite polarity to the primary magnetic field (Constable *et al.* 2009; Worzewski *et al.* 2010). The difference in TE and the corresponding 3-D response is evident for both ocean bottom and land sites; in comparison, the TM and the corresponding 3-D responses are in good agreement. The TM responses from the modelled sea are dominated by a galvanic charge build-up at the vertical ocean–land interface, providing a good approximation, even for 3-D structures. Given this, we decided to use TM mode responses that, as shown here, are robust even in 3-D situations.

We used a modified version of the code of Ogawa & Uchida (1996) for 2-D inversion, with modifications detailed below. The Ogawa and Uchida code used Rodi's (1976) algorithm (MOM's method) to calculate spatial derivatives on the ground. This method

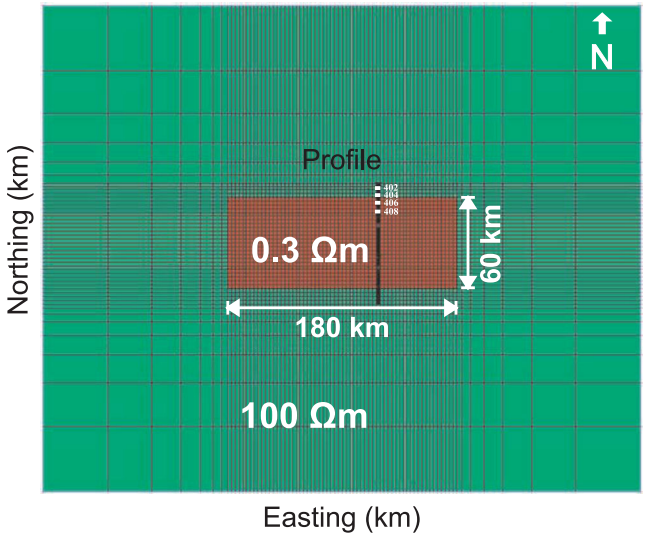

Figure 5. Initial models for 3-D and 2-D forward modelling tests. A box type (depth: 1.2 km, width: 60 km) bathymetry with 0.3 Ωm resistivity is set into the 100 Ωm half-space resistivity. White squares show the location of sites (402, 404, 406 and 408 from north to south) compared in Fig. 6.

is used for multiple levels of seafloors in this study. In addition, we modified the definition of roughness norm to include an *a priori* model in order to stabilize the inversion. The original roughness norm was $|Cm|^2$, where m is a model vector representing the log resistivity of the model, and C is the roughening matrix of the Laplacian operator. The modified version has a $|C(m - m_0)|^2$ norm, where m_0 is a vector comprising the log resistivity of the *a priori* model. The static shift was used as a constraint in inversion as in the original version of Ogawa & Uchida (1996) code.

We started with the initial model construction as described here. Initially, sea water was assigned a fixed value of 0.3 Ωm by referencing the bathymetric data. It is also important to include a sedimentary layer as *a priori* information, as we do not have the short-period data required to constrain the resistivity of shallow areas immediately under individual ocean bottom sites. During this study, we used the distribution of sediments identified using seismic reflection data (Carton *et al.* 2007), with Fig. 7 showing the shallow resistivity distribution that was incorporated into the model as a constraint. During modelling, a thick sedimentary layer was assigned a fixed resistivity of 10 Ωm, extending to a depth of 4–5 km below the ÇB (Okay *et al.* 2000; Carton *et al.* 2007), with the initial model having a uniform below-sediment resistivity. Error floor values of 10 per cent and 3° were used for apparent resistivity and phase values, respectively, with the initial model also used as an *a priori* model.

We formulated three initial models that used uniform below-sediment resistivities of 10, 100 and 1000 Ωm, with the final models dependent on the initial (*a priori*) models. Of the three initial models, the 100 Ωm model showed the best fit with the data, with root mean square misfit values of 2.1 and 1.9 for profiles P1 and P2, respectively.

The identified 2-D electrical resistivity structures in the eastern Marmara Sea along profiles P1 and P2 are shown in Figs 8(a) and (b). The electrical resistivity models have similar

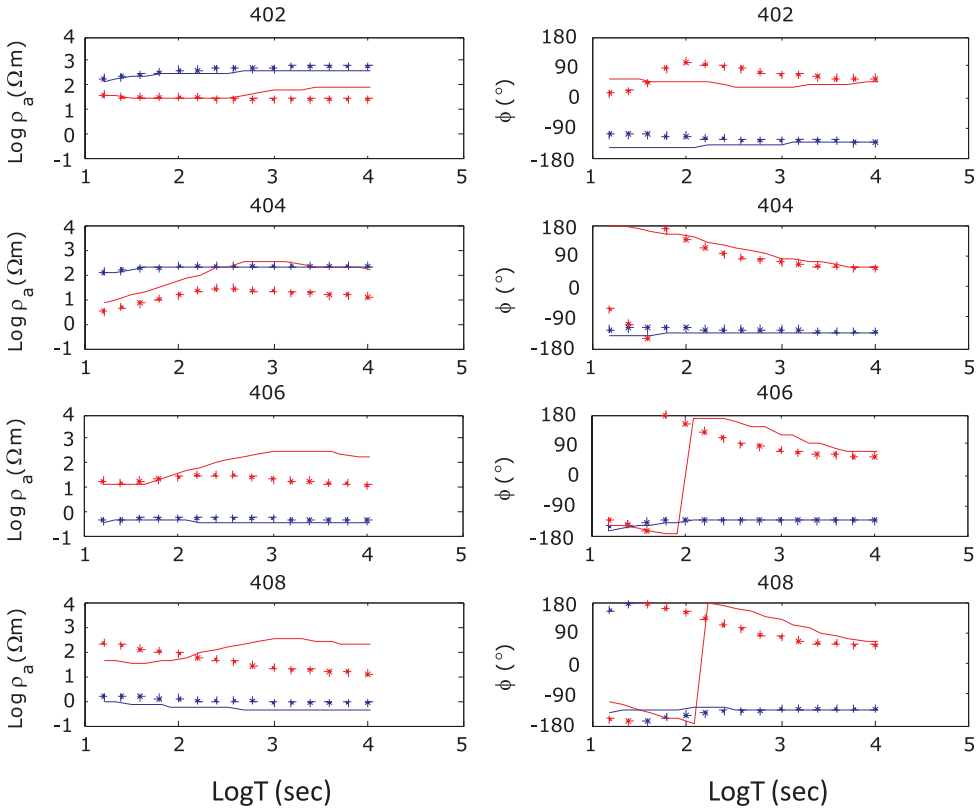

Figure 6. Apparent resistivity (left-hand column) and phase (right-hand column) responses of 3-D (asterisk) and 2-D (solid line) forward modelling are given for the northeast (blue) mode, which means electric field in the north and magnetic field in the east direction is used, and east–north (red) mode, the opposite case with the northeast mode. Since the model is symmetric, only sample sites (402, 404, 406 and 408) from north (top panel) to the centre (bottom panel) of the profile are shown. Robustness of the TM mode is clear especially for the longer periods.

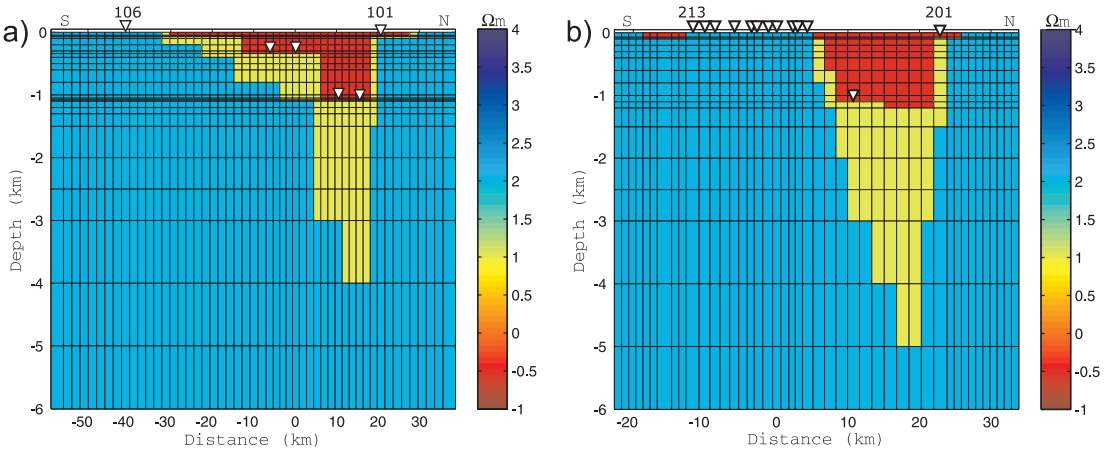

Figure 7. Initial models of P1 (a) and P2 (b) for 2-D inversion are shown up to 6 km. White rectangles represent the site locations. Bathymetry was fixed to 0.3 Ωm while underlying sediment was fixed to 10 Ωm. The resistivity of the half-space was set as 100 Ωm.

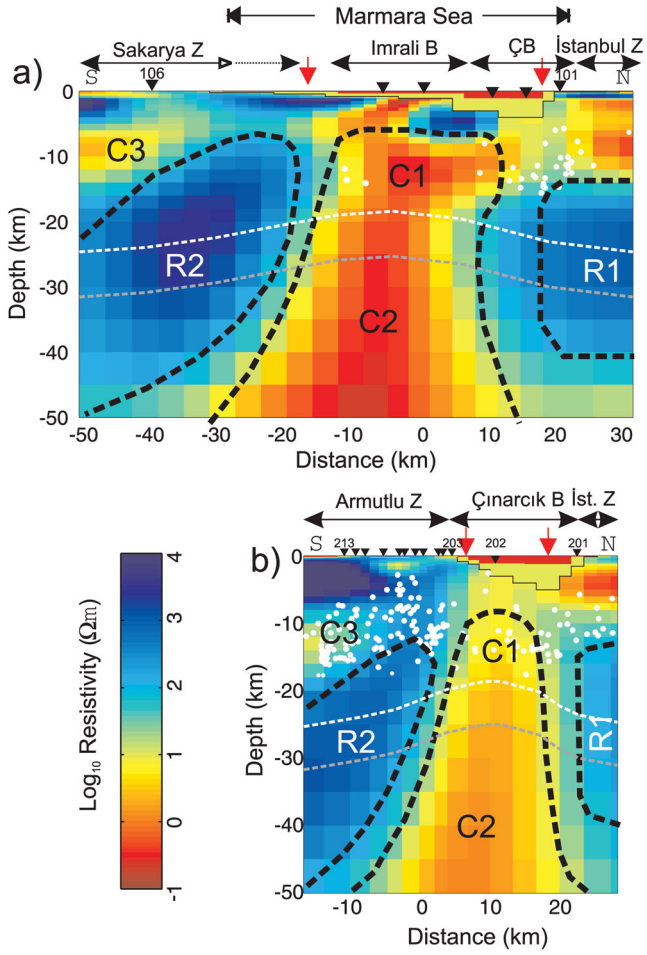

Figure 8. Final 2-D electrical resistivity models obtained from inversion of TM mode data for P1 (a) and P2 (b) profiles. Inverted triangles show site locations, red arrows indicate possible branches of the NAF, white circles represent microseismic activity from 2007 to 2010 (Bulut, GFZ) in and around the ÇB. Black line beneath the basins indicates depth of the fixed sediment in modelling. The white and grey dashed lines indicate the upper crust–lower crust boundary (brittle-ductile transition zone) and Moho depth (Laigle *et al.* 2008; Becel *et al.* 2010).

resistivity distributions beneath both profiles, with a shallow conductor (C1) starting a few kilometres beneath the sedimentary layer and merging with a deeper conductor (C2) in the central part of the profiles. Another shallow conductor (C3) in P1, located between two resistive layers, is also present beneath the Armutlu Peninsula in P2. Both models contain deep resistors that horizontally bound the deep C2 conductor in the north (R1) and in the south (R2). The shallow resistive layer underlain by a conductive anomaly (C3) beneath the Armutlu Peninsula was also observed in the previous MT study by Tank *et al.* (2003) in which the structures down to almost 20 km were investigated.

A comparison of observed and calculated responses is shown in Figs 9 and 10, for profiles P1 and P2, respectively. These curves

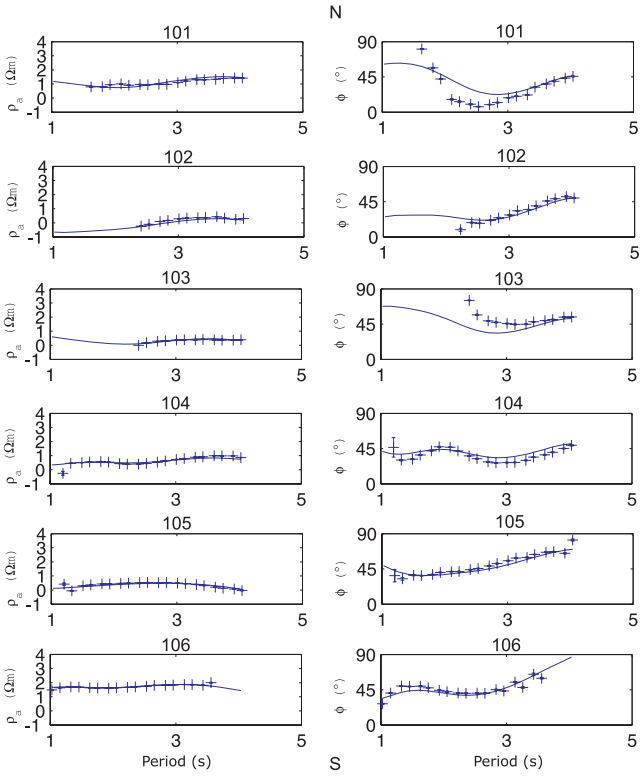

Figure 9. Fitting curves of the observed (plus sign) and calculated (straight line) data of P1 are demonstrated for sites from north (top panel) to south (bottom panel).

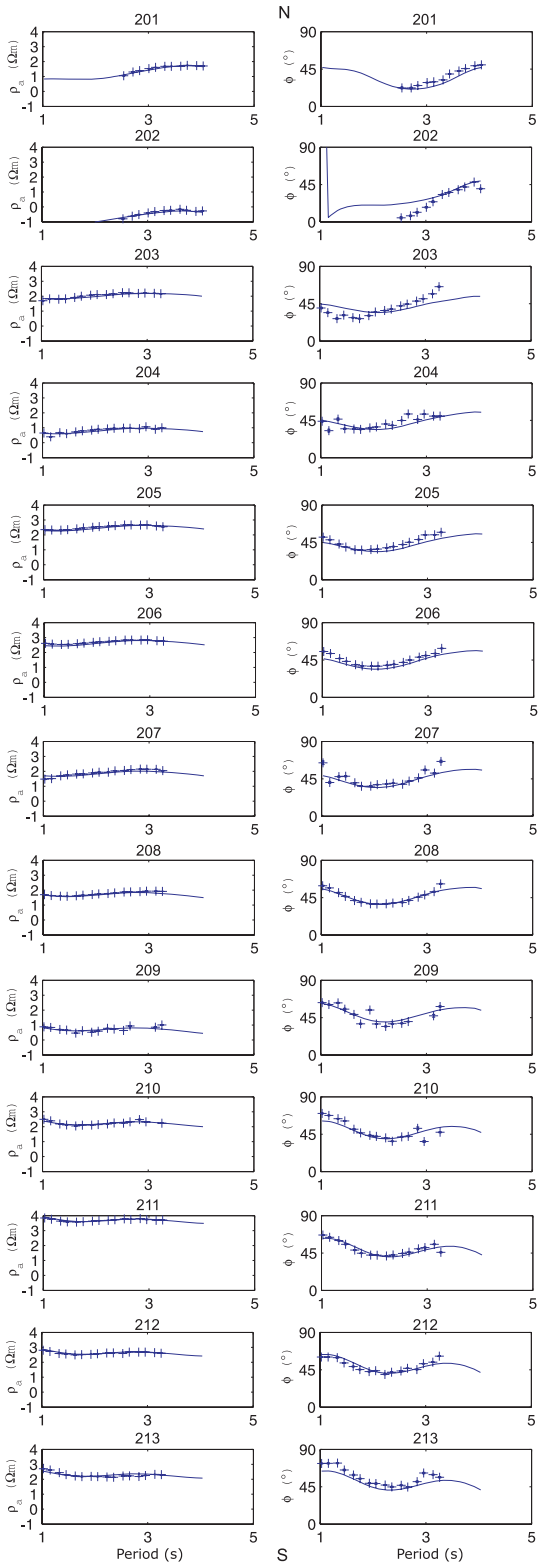

Figure 10. Fitting curves of the observed (plus sign) and calculated (straight line) data of P2 are demonstrated for sites from north (top panel) to south (bottom panel).

indicate a generally good recovery of the observed data. The apparent resistivity and phase responses are compared in pseudo-sections in Figs 11 and 12, confirming the recovery of the observed data.

We also tested the main features identified within the final models by forward modelling using resistivity changes. Figs 13 and 14 show sensitivity tests for the major anomalies [R1 (a), C1 (b), C2 (c) and R2 (d)] beneath profiles P1 and P2, respectively. These tests confirm that the modelling accurately represents the data. According to these tests, both conductive anomalies C1 and C2 in both profiles have resistivity values that range between 1 and 10 Ωm.

4 DISCUSSION

The results of this study provide the first electrical images of structures between the seafloor and the upper mantle beneath the Marmara Sea. The tectonic and geological implications of the major anomalies identified above are discussed in this next section.

4.1 Implications for tectonic configurations

The final models given in Figs 8(a) and (b) show three domains; one is consisting of two central subvertical conductors (C1, C2), and others including the surrounding resistors (R1, R2). This distribution is consistent with the known tectonic provinces in the study area. The northern resistor (R1) and the overlying 10-km-thick conductor which belong to the İstanbul–Zonguldak Zone represent Precambrian bedrock and Ordovician to Carboniferous sediments (Yılmaz *et al.* 1997). The southern resistor (R2) corresponds to the Sakarya and Armutlu zones, and represents Paleozoic metamorphic rocks of the Sakarya Continent. The zone with the subvertical conductive anomaly corresponds to the collision zone between the İstanbul–Zonguldak Zone and the Sakarya Continent.

4.2 Sources of conductive anomalies

4.2.1 Upper crustal conductor (C1)

An upper crustal shallow conductive anomaly, here named C1, is present in the middle of both profiles with a resistivity of 1–10 Ωm. Experimental data indicate that electrical resistivity of aqueous crustal fluids is in the range of 0.01–0.1 Ωm (Nesbitt 1993); meaning that, using the Hashin–Shtrikman upper bound (Hashin & Shtrikman 1962), a bulk resistivity of 1–10 Ωm can be explained by porosity of 0.15–15.0 per cent. In addition, a seismic tomography study detected low *Vp* and *Vp*/*Vs* ratio zones at depths of 5–15 km beneath the ÇB (Barış *et al.* 2005). These zones were also interpreted as areas of high-fluid content. The distribution of microseismic epicentres around the ÇB is shown in Fig. 1(b). In Fig. 8, projected hypocentres of earthquakes that were at a distance of ±10 km from the profiles P1 and P2 are given. This projection indicates a good correlation between resistivity and seismicity, with the majority of the microseismic activity clustering outside the rims of the C1 conductor beneath the profile P1, and close to the C1 and C3 conductors beneath the profile P2 (Fig. 8).

This configuration can be explained by the existence of an interconnected fluid network and the associated triggering of earthquakes by the migration of fluids into the surrounding crust. Migration of fluid into less-permeable crust can reduce the effective normal stress and trigger earthquakes (Sibson *et al.* 1988; Cox 1999; Sibson 2000). Such seismicity–resistivity relationships are known in a number of seismically active regions (Ogawa *et al.* 2001; Ogawa & Honkura 2004; Wannamaker *et al.* 2004, 2009; Jiracek *et al.* 2007; Mitsuhata *et al.* 2001).

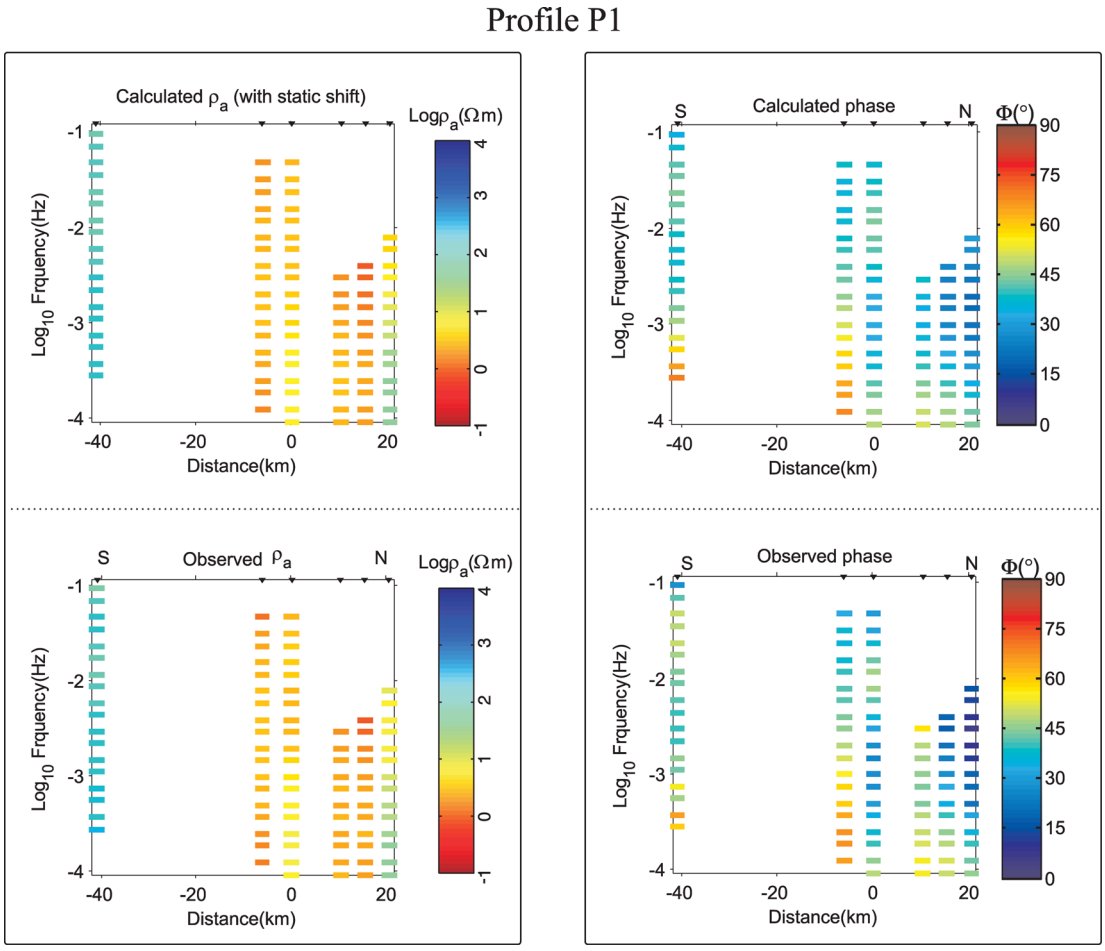

Figure 11. Calculated (top panel) and observed (bottom panel) apparent resistivity (left-hand panel) and phase (right-hand panel) pseudo-sections of P1 for TM mode.

4.2.2 Lower crust to upper-mantle conductor C2

The research discussed here identified a vertical conductor, here named C2, runs from the lower crust to the upper mantle. This conductor may be associated with the presence of high-salinity fluids and/or the partial melting of mantle material due to the asthenospheric upwelling. The bulk resistivity (1–10 Ωm) of the C2 zone indicates either 0.15–15.0 per cent fluid or 1.5–39 vol per cent melt fraction by the Hashin–Shtrikman upper bound, using pure melt and aqueous fluid resistivities of 0.1–0.3 and 0.01–0.1 Ωm, respectively (Presnall *et al.* 1972; Waff 1974; Tyburczy & Waff 1983; Nesbitt 1993; Yoshino *et al.* 2010; Pommier & LeTrong 2011; Evans 2012).

The presence of partial melt is supported by the upwelling of asthenospheric material by other magnetotelluric studies documented for the onland extent of the NAF (Gürer 1996; Tank *et al.* 2005; Türkoğlu *et al.* 2008). In addition, seismological studies indicate that the crustal thickness around the Marmara Sea varies between 29 and 32 km (Gürbüz *et al.* 2003; Zor *et al.* 2006). Within the Marmara Sea, it is almost 31 km (grey dashed line in Fig. 8), except areas to the south of the Central Basin and beneath the Çınarcık and İmralı basins. Here, the crustal thickness decreases to 26 km due to the thinning of the upper crust associated with lithospheric-scale extension (Laigle *et al.* 2008; Becel *et al.* 2009). In addition to that, Straub & Kahle (1994) documented a NE–SW oriented extensional regime along the northern branch of the NAF, in the present study area. Furthermore, the presence of regions with high heat flow (100–140 mW m^{-2}) in the Marmara Sea (İlkışık 1995; Tezcan 1995) and mantle-derived He (>50 per cent of total He concentration) along the west to central segment of the NAF (Güleç *et al.* 2002) may indicate the presence of zones with significant extension and high temperature that may be related to the upwelling of asthenospheric material. Dilek & Altunkaynak (2007, 2009) suggested partial melting as a source of the Eocene volcanism in and around the Marmara Sea; as well, Altunkaynak (2007) showed that the geochemistry of the Marmara granitoids was indicative of significant crustal contamination during magma ascent.

These data suggest that fluids are migrating from a deep ductile region to the upper brittle zone beneath the Marmara Sea. If this conductor does represent partial melting, one possibility is that the high temperatures, partial melting and fluid-releasing dehydration reactions documented in this area may be related to asthenospheric upwelling caused by subduction of Neo-Tethyan oceanic lithosphere beneath the Sakarya Continent, which was followed by slab breakoff.

The form of the deep C2 conductor changes beneath both profiles, with the conductor appearing narrower, but with a higher resistivity, beneath profile P2 than beneath profile P1. One possible reason for this is that profile P2 crosses the easternmost part of the ÇB and the Armutlu Peninsula, and does not intersect structures beneath the İmralı Basin which is associated with highly conductive aqueous fluids and/or molten crustal and mantle material. The basement

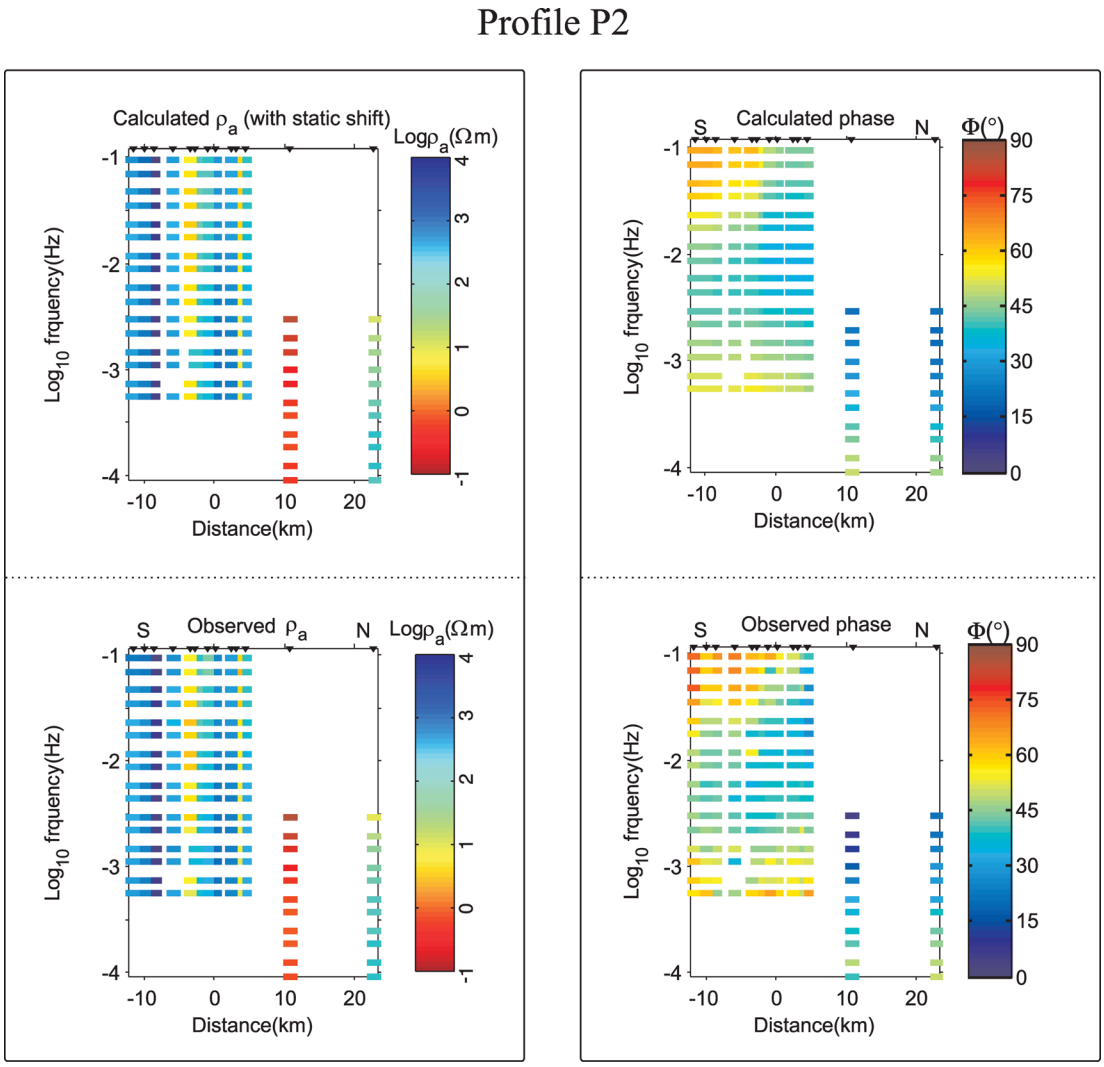

Figure 12. Calculated (top panel) and observed (bottom panel) apparent resistivity (left-hand panel) and phase (right-hand panel) pseudo-sections of P2 for TM mode.

rocks of the Armutlu Peninsula consist of a succession of high- and low-grade metamorphics overlain by sedimentary rocks—a similar lithological sequence to that found within the İstanbul–Zonguldak units and Sakarya Continent (Yılmaz and Tüysüz 1991; Yılmaz *et al.* 1995). This indicates that profile P1 includes structures beneath both the İmralı and ÇBs, leading to a wider conductive anomaly than observed in the profile P2.

Deep subvertical conductors beneath large strike-slip faults have also been recently imaged along the NAF (Tank *et al.* 2005), the Alpine Fault in New Zealand (Wannamaker *et al.* 2002) and the San Andreas Fault (Becken *et al.* 2011), suggesting that these conductors may be a common feature in areas containing major strike-slip faults. The existence of this type of conductor extending to 50-km depth below the NAF near İzmit was documented by Tank *et al.* (2005), who interpreted the deeper part of the conductor to be a region of partial melt, and the shallow part (just under the brittle–ductile transition) to be a region containing saline fluids. A similar interpretation, combining regions of fluid and underlying partial melt, was also provided in Tibet by Li *et al.* (2003). Wannamaker *et al.* (2002) and Becken *et al.* (2011), on the other hand, showed that deep vertical conductor is fluid source supplying crustal fluid.

4.3 Relationship with the NAF

4.3.1 Continuous tectonic features along the NAF

We have documented significant similarities between the features resolved in MT models obtained for the Marmara Sea area, and in models for the region to the east of the study area along the NAF. The Marmara Sea profiles, P1 and P2, are dominated by a conductor that is horizontally bounded by resistive zones to the north and south (Fig. 15). This structure was also observed in previous onshore MT studies in the eastern part of the present study area along the NAF (Gürer 1996; Honkura *et al.* 2000; Oshiman *et al.* 2002; Tank *et al.* 2005; Kaya *et al.* 2009; Kaya 2010). The distribution of geothermal fields from east to west along the NAF (Aydın *et al.* 2005) is also consistent with the location of the deep conductors, suggesting that similar structures may also be present along the western part of the NAF in the Marmara Sea area. In terms of extending geo-electrical structures from the eastern Marmara region to the ÇB, we suggest that, from north to south, the Istanbul–Zonguldak and Armutlu–Almacik zones and the Sakarya Continent tectonic zones are continuous from the previously documented onland areas to the area beneath the Marmara Sea.

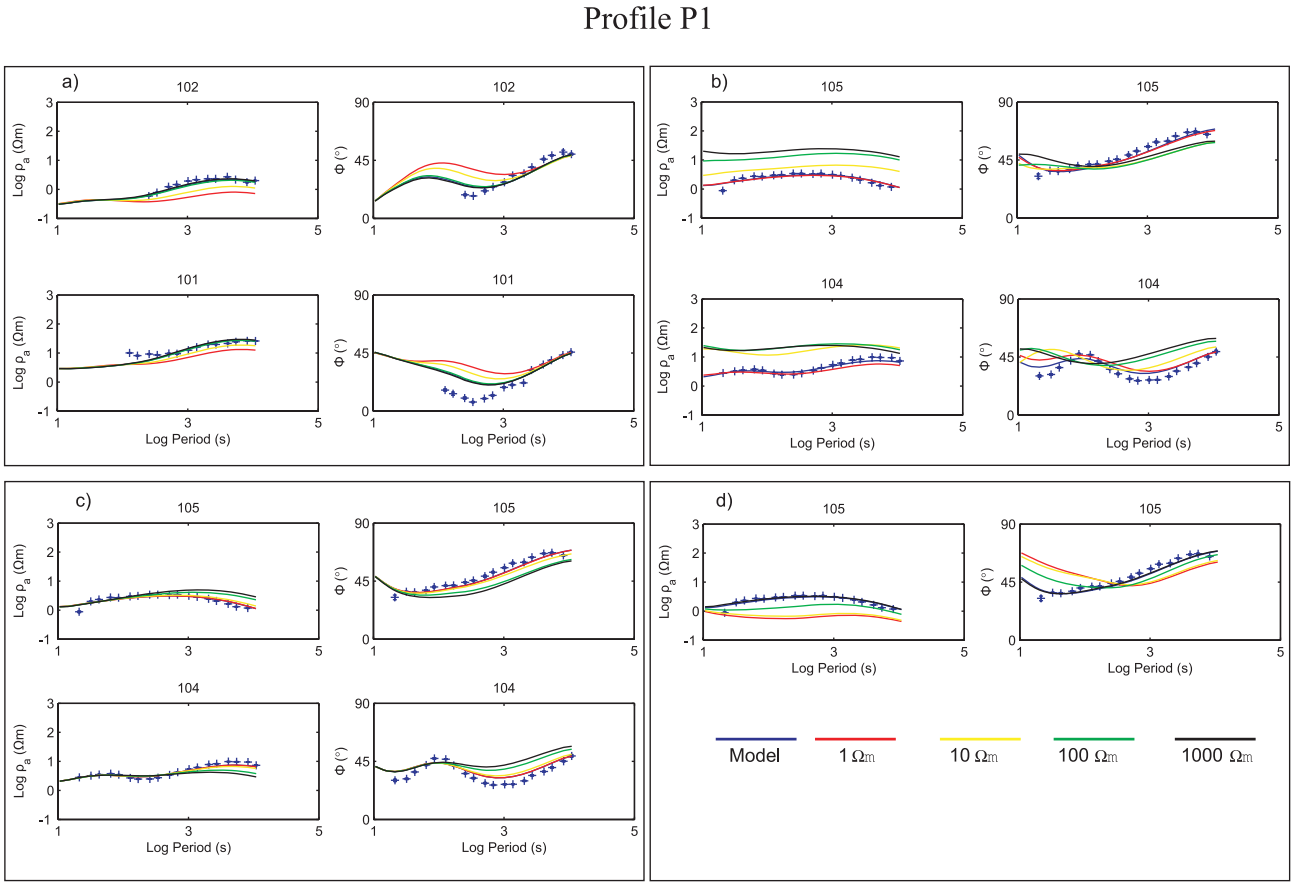

Figure 13. Resolution tests for the anomalies R1 (a), C1 (b), C2 (c) and R2 (d) of P1. The responses at the stations mostly sensitive to the anomalies are shown. Blue colour represents the model response while red, yellow, green and black colours show responses to the anomaly with 1, 10, 100 and 1000 Ωm, respectively. Plus sign (+) demonstrates the observed data. In all anomaly tests, best fit is obtained by model response.

4.3.2 Branches of the NAF

Previous MT studies identified a correlation between resistor–conductor boundaries and onland branches of the NAF (Tank *et al.* 2003, 2005; Kaya *et al.* 2009). In this respect, subvertical resistor–conductor boundaries beneath the Marmara Sea may also indicate the location of NAF branches, suggesting that the northern resistor–conductor boundary in the study area represents a northern branch of the NAF (NAF1) that extends west from the İzmit earthquake rupture zone to the Marmara Sea. Fig. 15 shows both extension of the NAF branches and resistivity distribution along the NAF from Düzce region to the Marmara Sea.

The second boundary, located at the southern escarpment of the ÇB beneath profile P2, is also observed beneath profile P1, suggesting that this minor branch of the NAF extends farther to the west. The boundary at the southern part of the C2 zone, beneath profile P1, implies the existence of another branch of the NAF, as shown by a dashed line in Figs 1 and 15. This has often been referred to as the middle branch though it is one strand of the southern branch of the NAF (Yilmaz *et al.* 2010). Here we refer to this branch as NAF2 which means the extension of the southern branch of the NAF in the Marmara Sea (Fig. 15). Extension of these subvertical resistor–conductor boundaries to at least 50 km depth suggests deeply rooted NAF that is also supplied by a teleseismic tomography study indicating a *P*-wave velocity contrast, represented by relatively high *P*-wave velocity perturbations (δVp) to the north of the NAF and low *P*-wave velocity perturbations to the south, down to a depth of 150 km in the Marmara Sea (Biryol *et al.* 2011). In order to improve our knowledge of the extension of these structures farther to the west, more OBEM instrument data from offshore areas to the west are required.

Resistivity structures defined around the rupture zones of the 1999 İzmit and Düzce earthquakes showed that the main shocks occurred within high-resistivity zones that were bounded to the south by lower-resistivity zones (Tank *et al.* 2003; Kaya *et al.* 2009). This suggests that along the NAF, comparisons between resistive structures beneath the Marmara Sea and the epicentres of the 1999 earthquakes may be crucial in relating high-resistivity zones to possible asperity zones that may initiate a large devastating event within the Marmara Sea, which is an area of increased seismicity after the İzmit earthquake. This indicates that more MT research needs to be undertaken on the resistive zone at sites farther to the north in the ÇB.

4.3.3 Tectonic models under the Marmara Sea

The single dextral strike-slip fault model in the Marmara Sea suggests westward extension of the northern branch of the NAF along the northern escarpment of the ÇB (Le Pichon *et al.* 2001) corresponding to the northern resistor–conductor boundary in our final models. In order to be able to support or decline continuation of a single fault in this model, more OBEM instrument data from offshore areas to the west are needed to figure out if there exists either many or a single resistivity boundary corresponding to the fault branch.

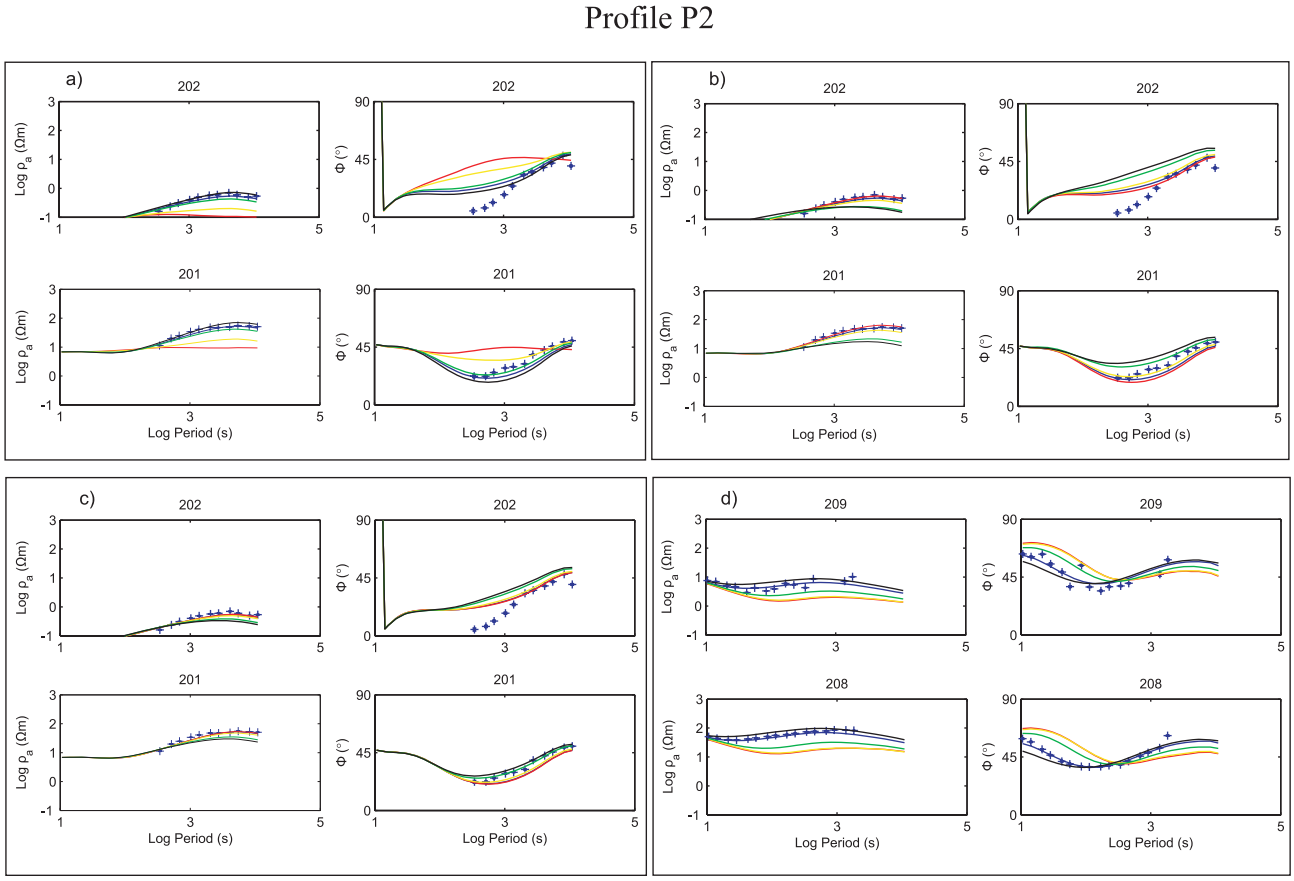

Figure 14. Resolution tests for the anomalies R1 (a), C1 (b), C2 (c) and R2 (d) of P2. The responses at the stations mostly sensitive to the anomalies are shown. Blue colour represents the model response while red, yellow, green and black colours show responses to the anomaly with 1, 10, 100 and 1000 Ωm, respectively. Plus sign (+) demonstrates the observed data. In all anomaly tests, best fit is obtained by model response.

The pull-apart model, on the other hand, suggests segmented faulting of the NAF due to both normal and strike-slip faulting regimes in the Marmara Sea (Armijo *et al.* 1999). The location of the branches of the NAF in the eastern Marmara Sea and extensional regime suggested by this model are supported by our resistivity models although it seems from our models that extension is not strictly limited to crustal scale as suggested by this model.

However, the crustal thinning model suggests both strike-slip and normal faulting where branches are consistent with resistivity boundaries in our models, and lithospheric scale extension in the Marmara Sea. The continuation of deep conductive material to shallow depths, as indicated by our electrical resistivity modelling, supports ongoing crustal thinning beneath the eastern Marmara Sea.

5 CONCLUSIONS

We performed 2-D modelling of MT data collected at both offshore and onshore sites along the western part of the NAF. Electrical resistivity models determined by 2-D inversions of TM mode data contain some characteristics related to the NAF. The presence of a conductor (C2) bounded by resistive blocks (R1 and R2) is similar to that previously documented in profiles crossing the İzmit earthquake rupture zone, and characterizes the western extension of the NAF from the east to the Marmara Sea. The resistor–conductor boundaries observed to the north and south of C2 correspond to the northern and southern branches of the NAF in the Marmara Sea, respectively. The shallow conductor C1, the presence of which implies the existence of a zone of interconnected pore fluid, seems to be related to microseismic activity through movement of fluids towards a more resistive seismic zone, whereas the deep conductor C2, which is probably related to the presence of fluid originating from dehydration and partial melt derived from upwelling of hot asthenospheric material, may be the source of a shallow interconnected fluid zone (i.e. C1). Resistive zones near resistive–conductive boundaries are potential sites for large earthquakes along branches of the NAF; in particular, the northern branch of the NAF may be likely to generate future large earthquakes beneath the Marmara Sea and as such requires further study.

ACKNOWLEDGEMENTS

This study was supported by KAKENHI (19253002). TK was supported by Monbukagakusho (Japanese Government) Scholarship. SBT was partly supported by the JSPS-PD fellowship program. We thank the Office of Navigation, Hydrography and Oceanography of the Turkish Naval Forces, and Turkish Airlines for their assistance during this study. We are grateful to the Marine Research Coordinating Office of the General Directorate of Mineral Research and Exploration (MTA) for providing bathymetry data for the Marmara Sea. We thank Dr. Fatih Bulut (GFZ) for sharing his high-resolution microseismic locations in and around the ÇB, and are grateful to Tadanori Goto and Elif Tolak for his help during instrument preparation. We also thank two anonymous reviewers and Dr. Gary Egbert for their valuable comments and contributions to this paper. Some

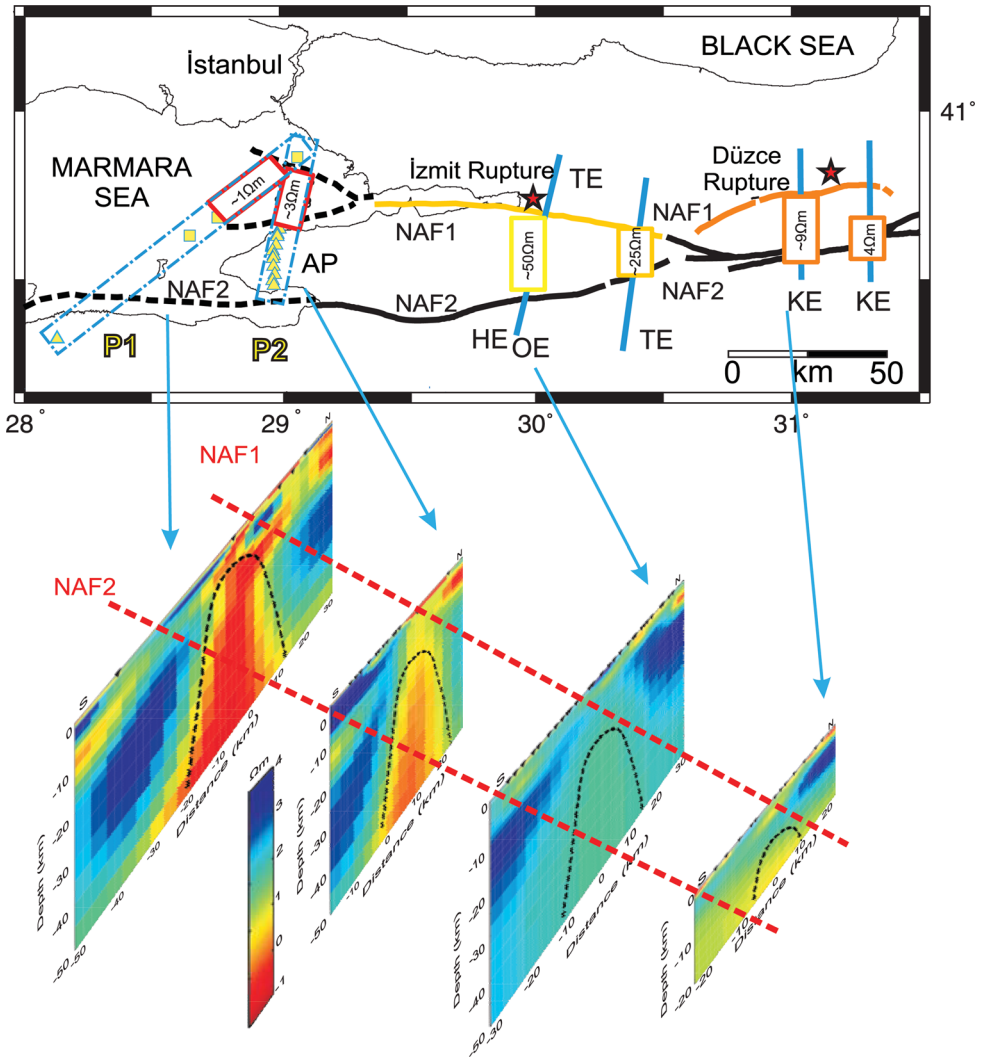

Figure 15. Upper panel: map showing resistivity variation at ~15 km depth across and along the NAF from the 1999 İzmit and Düzce earthquake rupture zones in the east to the Marmara Sea in the west. Red stars denote epicentres of the İzmit and Düzce earthquakes, blue lines indicate MT profiles and hot-coloured rectangles show the location of the conductors. Lower panel: from left- to right-hand side, 2-D resistivity models generated during this study and for two profiles crossing the İzmit and Düzce ruptures; resistivities are plotted in the same colour range. The presence of the middle conductor bounded by resistive zones from east to west in all profiles is indicative of the continuation of the NAF. NAF1, NAF Northern branch; NAF2, NAF Southern branch.

of the figures presented here were generated using the Generic Mapping Tools (GMT) code developed by Wessel & Smith (1995).

REFERENCES

Akyüz, H.S., Hartleb, R., Barka, A., Altunel, E., Sunal, G., Meyer, B. & Armijo, R., 2002. Surface rupture and slip distribution of the 12 November 1999 Duzce earthquake (*M* 7.1), North Anatolian Fault, Bolu, Turkey, *Bull. seism. Soc. Am.,* **92**(1), 61–66.

Altunkaynak, S., 2007. Collision-driven slab breakoff magmatism in northwestern Anatolia, Turkey, *J. Geol.,* **115,** 63–82.

Armijo, R., Meyer, B., Hubert, A. & Barka, A., 1999. Westward propagation of the North Anatolian Fault into the northern Aegean: timing and kinematics, *Geology,* **27,** 267–270.

Armijo, R., Meyer, B., Navarro, S. & King, G., 2002. Slip partitioning in the Sea of Marmara pullapart: a clue to propagation processes of the North Anatolian Fault, *Terra Nova,* **14,** 80–86.

Aydın, İ., Karat, H.İ. & Koçak, A., 2005. Curie-point depth map of Turkey, *Geophys. J. Int.,* **162,** 633–640.

Barış, Ş., Nakajima, J., Hasegawa, A., Honkura, Y., Ito, A. & Üçer, S.B., 2005. Three-dimensional structure of Vp, Vs and Vp/Vs in the upper crust of the Marmara region, NW Turkey, *Earth Planets Space,* **57,** 1019–1038.

Barka, A.A., 1992. The North Anatolian fault zone, *Annales Tectonicae,* **6,** 164–195.

Becel, A. *et al.*, 2009. Moho, crustal architecture and deep deformation under the North Marmara Trough, from the SEISMARMARA Leg 1 offshore-onshore reflection-refraction survey, *Tectonophysics,* **467,** 1–21.

Becken, M., Ritter, O., Bedrosian, P.A. & Weckmann, U., 2011. Correlation between deep fluids, tremor and creep along the San Andreas Fault, *Nature,* **480,** 87–90.

Biryol, C.B., Beck, S.L., Zandt, G. & Özaçar, A.A., 2011. Segmented African lithosphere beneath the Anatolian region inferred from teleseismic P-wave tomography, *Geophys. J. Int.,* **184,** 1037–1057.

Bulut, F., Bohnhoff, M., Ellsworth, W.L., Aktar, M. & Dresen, G., 2009. Microseismicity at the North Anatolian Fault in the Sea of Marmara offshore İstanbul, NW Turkey, *J. geophys. Res.,* **114,** doi:10.1029/2008JB006244.

Carton, H. *et al.*, 2007. Seismic imaging of the three-dimensional architecture of the Çınarcık Basin along the North Anatolian Fault, *J. geophys. Res.,* **112,** B06101, doi:10.1029/2006JB004548.

Chave, A.D., Thomson, D.J. & Ander, M.E., 1987. On the robust estimation of power spectra, and transfer functions, *J. geophys. Res.,* **92**(B1), 633–648.

Chouteau, M. & Tournerie, B., 2000. Analysis of magnetotelluric data showing phase rolling out of quadrant (PROQ), *SEG Expand. Abstr.,* **19,** 344–346.

Constable, S., Key, K. & Lewis, L., 2009. Mapping offshore sedimentary structure using electromagnetic methods and terrain effects in marine magnetotelluric data, *Geophys. J. Int.,* **176,** 431–442.

Cox, S.F., 1999. Deformational controls on the dynamics of fluid flow in mesothermal gold systems, in *Fractures, Fluid Flow and Mineralization,* Vol. 155, pp. 123–140, eds McCaffrey, K.J.W., Lonergan, L. & Wilkinson, J.J., Geol. Soc. Lond. Spec. Pub.

Dilek, Y. & Altunkaynak, S., 2007. Cenozoic crustal evolution and mantle dynamics of post-collisional magmatism in western Anatolia, *Int. Geol. Rev.,* **49,** 431–453.

Dilek, Y. & Altunkaynak, S., 2009. Geochemical and temporal evolution of Cenozoic magmatism in western Turkey: mantle response to collision, slab break-off, and lithospheric tearing in an orogenic belt, *Geol. Soc.,* **311,** 213–233.

Evans, R.L., 2012. Chapter 3, Earth's electromagnetic environment, in *The Magnetotelluric Method, Theory and Practice,* eds Chave, A.D. & Jones, A.G., Cambridge University Press.

Groom, R.W. & Bailey, R.C., 1989. Decomposition of magnetotelluric impedance tensor in the presence of local three-dimensional galvanic distortion, *J. geophys. Res.,* **94,** 1913–1925.

Güleç, N., Hilton, D.R. & Mutlu, H., 2002. Helium isotope variations in Turkey: relationship to tectonics, volcanism and recent seismic activities, *Chem. Geol.,* **187,** 129–142.

Gürbüz, C., Bekler, T., Toksöz, M.N., Kuleli, S., Kalafat, D. & Schultz, C.A., 2003. Seismic refraction studies and crustal structure in Anatolia. Commission on controlled-source seismology: deep seismic methods, in Proceedings of the 12th International Workshop, Mountain Lake, 8–11 October 2003, Virginia, USA.

Gürer, A., 1996. Deep conductivity structure of the North Anatolian Fault Zone and the Istanbul and Sakarya Zones along the Golpazari-Akcaova profile, Northwest Anatolia, *Int. Geol. Rev.,* **38,** 727–736.

Hashin, Z. & Shtrikman, S., 1962. On some variational principles in anisotropic and nonhomogeneous elasticity, *J. Mech. Phys. Solids,* **10,** 335–342.

Honkura, Y. *et al.*, 2000. Preliminary results of multidisciplinary observations before, during and after the Kocaeli (İzmit) earthquake in the western part of the North Anatolian Fault Zone, *Earth Planets Space,* **52,** 293–298.

Hubert-Ferrari, A., Barka, A., Jacques, E., Nalbant, S., Meyer, B., Armijo, R., Tapponier, P. & King, G.C.P., 2000. Seismic hazard in the Marmara Sea region following the 17 August 1999 Izmit earthquake, *Nature,* **404,** 269–273.

İlkışık, O.M., 1995. Regional heat flow in western Anatolia using silica temperature estimates from thermal springs, *Tectonophysics,* **244,** 175–184.

Jiracek, G.R., Gonzalez, V.M., Caldwell, T.G., Wannamaker, P.E & Kilb, D., 2007. Seismogenic, Electrically Conductive, and Fluid Zones at Continental Plate Boundaries in New Zealand, Himalaya, and California-USA, in *A Continental Boundary: Tectonics at South Island, New Zealand.* Geophys. Monogr. Ser, Vol. 175, pp. 75–94, eds Okaya, D., Stern, T. & Davey, F.A., AGU, Washington, DC.

Karabulut, H., Özalaybey, S., Taymaz, T. & Aktar, M., 2003. A tomographic image of the shallow crustal structure in the Eastern Marmara, *Geophys. Res. Lett.,* **30,** doi:10.1029/2003GL018074.

Kasaya, T. & Goto, T., 2009. A small ocean bottom electromagnetometer and ocean bottom electrometer system with an arm-folding mechanism (Technical Report), *Explor. Geophys.,* **40,** 41–48.

Kaya, C., 2010. Deep crustal structure of northwestern part of Turkey, *Tectonophysics,* **489,** 227–239.

Kaya, T., Tank, S.B., Tunçer, M.K., Rokityansky, I.I., Tolak, E. & Savchenko, T., 2009. Asperity along the North Anatolian Fault imaged by magnetotellurics at Düzce, Turkey, *Earth Planets Space,* **61,** 871–884.

Ketin, İ., 1948. Über die tektonisch-mechanischen Folgerungen aus den grossen anatolischen Erdbeben des letzten Dezenniums, *Geol. Rund.,* **36,** 77–83.

Laigle, M., Becel, A., de Voogd, B., Hirn, A., Taymaz, T. & Özalaybey, S., the Members of the SEISMARMARA Leg1, 2008. A first deep seismic survey in the Sea of Marmara: whole crust and deep basins, *Earth planet. Sci. Lett.,* **270,** 168–179.

Le Pichon, X. *et al.*, 2001. The active Main Marmara Fault, *Earth planet. Sci. Lett.,* **192,** 595–616.

Li, S., Unsworth, M.J., Booker, J.R., Wei, W., Tan, H. & Jones, A.G., 2003. Partial melt or aqueous fluid in the mid-crust of Southern Tibet? Constraints from INDEPTH magnetotelluric data, *Geophys. J. Int.,* **153,** 289–304.

Mackie, R.L., Smith, J.T. & Madden, T.R., 1994. Three-dimensional electromagnetic modeling using finite difference equations: the magnetotelluric example, *Radio Sci.,* **29**(4), 923–935.

McKenzie, D., 1972. Active tectonics of the Mediterranean region, *Geophys. J. R. astr. Soc.,* **30,** 109–185.

McNeice, G.W. & Jones, A.G., 2001. Multisite, multifrequency tensor decomposition of magnetotelluric data, *Geophysics,* **66**(1), 158–173.

Mitsuhata, Y., Ogawa, Y., Mishina, M., Kono, T., Yokokura, T. & Uchida, T., 2001. Electromagnetic heterogeneity of the seismogenic region of 1962 M6.5 Northern Miyagi Earthquake, northeastern Japan, *Geophys. Res. Lett.,* **28,** 4371–4374.

Nesbitt, B.E., 1993. Electrical resistivities of crustal fluids, *J. geophys. Res.,* **98,** 4301–4310.

Ogawa, Y. & Honkura, Y., 2004. Mid-crustal electrical conductors and their correlations to seismicity and deformation at Itoigawa-Shizuoka Tectonic Line, Central Japan, *Earth Planets Space,* **56,** 1285–1291.

Ogawa, Y. & Uchida, T., 1996. A two-dimensional magnetotelluric inversion assuming Gaussian static shift, *Geophys. J. Int.,* **126,** 69–76.

Ogawa, Y. *et al.*, 2001. Magnetotelluric imaging of fluids in intraplate earthquake zones, NE Japan back arc, *Geophys. Res. Lett.,* **28,** 3741–3744.

Okay, A.I., Kaşlılar-Özcan, A., İmren, C., Boztepe-Güney, A., Demirbağ, E. & Kuşçu, İ., 2000. Active faults and evolving strike-slip basins in the Marmara Sea, northwest Turkey: a multichannel seismic reflection study, *Tectonophysics,* **321,** 189–218.

Oshiman, N., 2002. Deep resistivity structure around the fault associated with the 1999 Kocaeli earthquake, Turkey, in *Seismotectonics at the Convergent Plate Boundary,* pp. 293–303, eds Fujinawa, Y. & Yoshida, A. *et al.*, Terra Sci. Publ. Company, Tokyo.

Örgülü, G., 2010. Seismicity and source parameters for small-scale earthquakes along the splays of the North Anatolian Fault (NAF) in the Marmara Sea, *Geophys. J. Int.,* **184,** 385–404.

Pınar, A. *et al.*, 2010. Spatial variation of the stress field along the fault zone of the 1999 İzmit earthquake, *Earth Planets Space,* **62,** 237–256.

Pommier, A. & LeTrong, E., 2011. "SIGMELTS": a web portal for electrical conductivity calculations in geosciences, *Comput. Geosci.,* **37**(9), doi:10.1016/j.cageo.2011.01.002.

Presnall, D.C., Simmons, C.L. & Porath, H., 1972. Change of electrical conductivity of a synthetic basalt during melting, *J. geophys. Res.,* **77,** 5665–5672.

Ritter, O., Hoffmann-Rothe, A., Bedrosian, P.A., Weckmann, U. & Haak, V., 2005. Electrical conductivity images of active and fossil fault zones, in *High Strain Zones: Structure and Physical Properties,* Vol. 245, pp. 165–186, eds Bruhn, D.F. & Burlini, L., Special Publication, Geol. Soc. London.

Rodi, W.L., 1976. A technique for improving the accuracy of finite element solutions for Magnetotelluric data, *Geophys. J. R. astr. Soc.,* **44,** 483–506.

Şengör, A.M.C., Tüysüz, O., İmren, C., Sakınç, M., Eyidoğan, H., Görür, N., Le Pichon, X. & Rangin, C., 2005. The North Anatolian Fault: a new look, *Annu. Rev. Earth planet. Sci.,* **33,** 37–112.

Sibson, R.H., 2000. Fluid involvement in normal faulting, *J. Geodyn.,* **29,** 469–499.

Sibson, R.H., Roberts, F. & Paulson, K.H., 1988. High-angle reverse faults, fluid-pressure cycling and mesothermal gold deposits, *Geology,* **16,** 551–555.

Straub, C. & Kahle, H.G., 1994. Active crustal deformation in the Marmara Sea region, NW Anatolia, inferred from GPS measurements, *Geophys. Res. Lett.,* **22**(18), 2533–2536.

Tank, S.B., 2012. Fault Zone Conductors in Northwest Turkey inferred from audio frequency magnetotellurics, *Earth Planets Space,* **64,** 729–742.

Tank, S.B. *et al.*, 2003. Resistivity structure in the western part of the fault rupture zone associated with the 1999 İzmit earthquake and its seismogenic implication, *Earth Planets Space,* **55,** 437–442.

Tank, S.B. *et al.*, 2005. Magnetotelluric imaging of the fault rupture area of the 1999 İzmit (Turkey) earthquake, *Phys. Earth planet. Inter.,* **150,** 213–225.

Tezcan, A.K., 1995. Geo-thermal explorations and heat flow in Turkey, in *Terrestrial Heat Flow and Geothermal Energy in Asia,* pp. 23–42, eds Gupta, M.L. & Yamano, M., Oxford and IBH Publishing Co., Rotterdam.

Toksöz, M.N., Shakal, A.F. & Micheal, A.J., 1979. Space-time migration of earthquakes along the North Anatolian Fault and seismic gaps, *Pure appl. Geophys.,* **117,** 1258–1270.

Türkoğlu, E., Unsworth, M., Cağlar, İ., Tuncer, V. & Avşar, Ü., 2008. Lithospheric structure of the Arabia-Eurasia collision zone in eastern Anatolia: magnetotelluric evidence for widespread weakening by fluids? *Geology,* **36,** 619–622.

Tyburczy, J.A. & Waff, H.S., 1983. Electrical conductivity of molten basalt and andesite to 25 kilobars pressure: geophysical significance and implications for charge transport and melt structure, *J. geophys. Res.,* **88,** 2413–2430.

Unsworth, M., Bedrosian, P., Eisel, M., Egbert, G. & Siripunvaraporn, W., 2000. Along strike variations in the electrical structure of the San Andreas Fault at Parkfield, California, *Geophys. Res. Lett.,* **27**(18), 3021–3024.

Vozoff, K., 1991. The magnetotelluric method, in *Electromagnetic Methods in Applied Geophysics,* Vol. 2B, pp. 641–711, ed. Nabighian, M.N., Soc. Expl. Geophys., Tulsa, Oklahoma.

Waff, H.S., 1974. Theoretical consideration of electrical conductivity in a partially molten mantle and implications for geothermometry, *J. geophys. Res.,* **79,** 4003–4010.

Wannamaker, P.E., Hohmann, G.W. & Ward, S.H., 1984. Magnetotelluric responses of three-dimensional bodies in layered earths, *Geophysics,* **49,** 1517–1534.

Wannamaker, P.E., Jiracek, G.R., Stodt, J.A., Caldwell, T.G., Gonzalez, V.M., McKnight, J.D. & Porter, A.D., 2002. Fluid generation and pathways beneath an active compressional orogen, the New Zealand Southern Alps, inferred from magnetotelluric data, *J. geophys. Res.,* **107**(B6), doi:10.1029/2001BJ000186.

Wannamaker, P.E., Caldwell, T.G., Doerner, W.M. & Jiracek, G.R., 2004. Fault zone fluids and seismicity in compressional and extensional environments inferred from electrical conductivity: the New Zealand Southern Alps and U. S. Great Basin, *Earth Planets Space,* **56,** 1171–1176.

Wannamaker, P.E. *et al.*, 2009. Fluid and deformation regime of an advancing subduction system at Marlborough, New Zealand, *Nature,* **460,** 733–736.

Wessel, P. & Smith, W.H.F., 1995. New version of the generic mapping tools, *EOS, Trans. Am. geophys. Un.,* **76,** 329.

Worzewski, T., Jegen, M., Kopp, H., Brasse, H. & Castillo, W.T., 2010. Magnetotelluric image of the fluid cycle in the Costa Rican subduction zone, *Nat. Geosci.,* **4,** 108–111.

Yılmaz, Y. & Tüysüz, O., 1991. Anatomy of an imbricated zone: geology of the Kargı massif, Central Pontides, *Bull. Tech. Univ. İstanbul,* **44**(1–2), 279–299.

Yılmaz, Y., Gökaşan, E. & Erbay, A.A., 2010. Morphotectonic development of the Marmara Region, *Tectonophysics,* **488,** 51–71.

Yılmaz, Y., Genç, S.C., Yiğitbaş, E., Bozcu, M. & Yılmaz, K., 1995. Geological evolution of the late Mesozoic continental margin, Northwestern Anatolia, *Tectonophysics,* **243,** 155–171.

Yılmaz, Y., Tüysüz, O., Yiğitbaş, E., Genç, C. & Şengör, A.M.C., 1997. Geology and tectonic evolution of the pontides, in *Regional and Petroleum Geology of the Black Sea and Surrounding Region,* Vol. 68, pp. 183–226, ed. Robinson, A.G., AAPG Memoir, Tulsa, Oklahoma.

Yoshino, T., Laumonier, M., McIsaac, E. & Katsura, T., 2010. Electrical conductivity of basaltic and carbonatite melt-bearing peridotites at high pressures: implications for melt distribution and melt fraction in the upper mantle, *Earth planet. Sci. Lett.,* **295**(3–4), 593–602.

Zor, E., Özalaybey, S. & Gürbüz, C., 2006. The crustal structure of the eastern Marmara region, Turkey by teleseismic receiver functions, *Geophys. J. Int.,* **167,** 213–222.